SCIENTIFIC REPORTS

OPEN

SUBJECT AREAS:
METAMATERIALS
MATERIALS FOR OPTICS

Received
14 November 2013

Accepted
14 April 2014

Published
9 May 2014

Correspondence and requests for materials should be addressed to X.C. (xinchen@mail.sitp.ac.cn)

Vapor-deposited amorphous metamaterials as visible near-perfect absorbers with random non-prefabricated metal nanoparticles

Yun Zhang, Tiaoxing Wei, Wenjing Dong, Kenan Zhang, Yan Sun, Xin Chen & Ning Dai

National Laboratory for Infrared Physics, Shanghai Institute of Technical Physics, Chinese Academy of Sciences, Shanghai 200083, China.

Spatial order or periodicity is usually required and constructed with tens of nanometers in the feature size, which makes it difficult to process the near-perfect metamaterial absorbers (PMAs) working in the visible range in large-area and mass-production scale. Although many established technologies and theoretical modeling methods used for order-based metamaterials, aperiodic or disordered structures have been gradually recognized to achieve similar functionalities for which the ordered structures are overwhelmingly used. Here, we demonstrated the vapor-deposited 'amorphous' metamaterials as controlled-reflectance surfaces and tunable PMAs without the use of the lithographically ordered arrays, the prefabricated colloidal metal nanoparticles (MNPs) or the multilayer of nanoparticles. The flexible construction, the control of the monolayer of MNPs and the atomic-layer-deposited (ALD) dielectric spacer layer provide more insight for understanding the controlled-reflectance surfaces. Such processes have a few key advantages of CMOS-compatible simple processing, low cost and large-area plating, allowing the PMAs to be flexibly constructed in mass-production scale.

Metamaterials, an arrangement of artificial sub-wavelength structures have created extraordinary transmission[1], near-perfect absorption[2–6] and negative refraction[7–10] by tuning the optical transmission, absorption, scattering and interference. A variety of concepts and constructions for metamaterials have emerged and shown great promise in super-lens[11], sensors[12], detectors[13] and even invisible cloaking devices[14]. The manipulation on effective permittivity and permeability by structured design is the physical essence behind metamaterials. Spatial order or periodicity is usually required in metamaterials for the manipulation of the phase and the flow of wave by tuning effective permittivity and permeability. Although many established technologies and theoretical modeling methods have been used for order-based metamaterials, the goal of attaining metamaterials in a flexible non-lithographic way has yet to be achieved[15,16]. Recent advances on disordered photonics reveal that aperiodic or disordered structures have been gradually recognized to achieve similar functionalities for which the ordered structures are overwhelmingly used[15,17–21] Yan and Hedayati have separately proposed and confirmed the sandwich structures involving a multilayer[22–24] or a monolayer[25] of metal nanoparticles (MNPs) by coating, sputtering or thermal deposition processes towards the superior broadband absorption. All those demonstrate that the random non-prefabricated nanostructures can function as PMAs in simplified architectures without the need for extra lithographical and prefabrication process. ALD is one powerful surface nano-engineering technique[26,27] and has also demonstrated practical capability in the controlled interface in microelectronics and photovoltaics. Here, we show that neither ordered lithographical nanostructures nor self-assembled colloidal MNPs are necessary to attain the controllable metamaterials as controlled-reflectance surfaces or tunable PMAs working in the visible range. The controllable ALD dielectric oxide layer can identify the interference absorption while the lower surface coverage, uniform shapes and small sizes of the random non-prefabricated Au nanoparticles (Au-NPs) lead to the separable absorption peaks and ignorable scattering. The ALD dielectric layer and the random non-prefabricated MNPs have a few key advantages of CMOS-compatible simple processing, low cost and large-area plating, allowing the vapor-deposited controlled-reflectance surfaces or tunable PMAs to be flexibly constructed in mass-production scale.

Within a traditional PMA construction there are many different layers with interrelated roles and having different tolerance for fabrication processes and feature sizes. Ordered nanostructures are generally required and constructed with tens of nanometers in the feature size by electronic beam lithography or focused ion beam, which makes it difficult to process the PMAs working in the visible range (visible-PMAs) in large-area and mass-production scale. Thus, any architecture which is easy and flexible to process are desirably adopted, with the aim of delivering large-area controllable PMAs[3], in particular visible-PMAs. Evolved from the traditional PMAs[2–6] and the broadband PMAs[22–25], the metasurface with film-coupled colloidal MNPs, instead of lithographically ordered metal nanostructures, have recently been used to deliver the isotropic visible-PMAs[15], which has demonstrated that the ordered patterning or the multilayer of MNPs is not required for the fabrication of PMAs. Now, the question is whether both the lithographical processes and the prefabricated colloids can be simultaneously replaced by a simple and flexible vapor deposition for the controlled-reflectance surfaces or tunable PMAs with separable absorption.

Here, as a means of creating 'amorphous' metamaterials with the monolayer of MNPs as visible-PMAs without the use of lithographically ordered arrays and prefabricated colloidal MNPs, we use vapor deposited dielectric layer and random non-prefabricated MNPs. Furthermore, the flexible construction and the control of the monolayer of MNPs, the ALD dielectric spacer layer and the bottom metal layer provide more insight for understanding the PMAs. In Fig. 1a we show an illustration of the vapor-deposited PMAs with randomly-distributed and non-prefabricated metal nanostructures, along with the cross-sectional view of the real construction (see Fig. 1b). From the bottom, the PMAs is constructed on silicon or silica substrates coated with a dense and continuous metal (e.g. Ag here) thin film (labeled as metal I in Fig. 1a) of tens of nanometers in thickness by physical vapor deposition (e.g. thermal vapor deposition or sputtering coating). This opaque bottom layer effectively eliminates the transmission and reflects most of the incident waves. A dielectric layer of oxides (e.g. ZnO or Al_2O_3) as a spacer is then deposited on the metal I layer by ALD[26,27]. The monolayer of random and non-prefabricated metal (e.g. Au here) nanoparticles (labeled as metal II in Fig. 1a) as the top layer are formed by a thermal annealing process from the metal II layer pre-deposited on the oxide spacer layer. The annealing process ensures the formation of the metal II nanoparticles. Careful observations on Fig. 1 and Fig. S1 reveal that the Au nanoparticles (Au-NPs) are randomly distributed and present on the oxide spacer layer with a flat contact area formed during the annealing process. The flat contact area is beneficial for near-perfect absorbers because it leads to more effective magnetic surface current density to offset the electric surface current density from the incident waves[15]. The total surface coverage, obtained with the 3 nm thick annealed Au films on the ZnO films, is ~22% for the Au-NPs with a size distribution centered at ~50 nm, according to the statistical distribution of the contacting-area fraction of the Au-NPs (Fig. S1).

In Fig. 2, we compare the experimental and simulated absorptance (A) of the resulting vapor-deposited PMAs. The experimental absorptance spectra (Fig. 2a) was derived by $A = 1\text{-}R$ from the reflection (R) spectra. The bottom opaque Ag layer of about 70 nm in thickness is thick enough to eliminate the optical light transmission (T). The experimental absorptance (the black solid line) reaches over 99% at near normal incidence (8 degree off the surface normal) at the wavelength of 670 nm, along with an absorptance of more than 80% at ~500 nm. In plasmonic metal nanostructures as PMAs, it is essential to simultaneously minimize the reflectance and the transmittance of the medium. It is rather difficult to eliminate the reflection at a special wavelength although the transmission is relatively easy to be reduced. For the PMAs, the reflection coefficients r_s for the s polarization can be described as

$$r_s = \frac{z_{eff} \times \cos(\theta_i) - z_0 \times cos(\theta_t)}{z_{eff} \times \cos(\theta_i) + z_0 \times cos(\theta_t)}, \quad (1)$$

where θ_i and θ_t are the incident and the transmitted angles of the electromagnetic wave with respect to the surface normal, respectively. $z_0 = \sqrt{\mu_0/\varepsilon_0}$ is the impedance of the media (i.e. air) while z_{eff} is the effective impedance of the PMA. Once $z_{eff} = 0$, $r_s = -1$, corresponding to the case that the incident light hits on a solid 'electric wall', for $z_{eff} = \infty$, on the other hand, $r_s = +1$ indicates that the incident light is reflected by a 'magnetic wall'[28]. Thus, a suitable effective impedance could lead to $r_s = 0$, i.e. the reflectionless case, which is the fundamental idea for PMAs and can be realized by carefully tuning the dielectric spacer and the top layer formed by a monolayer of MNPs.

The numerical simulations by finite difference time domain (FDTD) algorism were performed by employing a uniform semi-spherical nanoparticle array with a particle size of 50 nm, a periodicity of 94 nm, as well as a total surface coverage of 22%. The permittivity of the ZnO spacer layer was set to be 4 and that of the Au-NPs was obtained from the literature[29]. We noted that the permittivity of Ag film in the real system should have a larger imaginary part than that of the bulk Ag due to the surface scattering and the grain boundaries[12,30]. A careful comparison of the experimental and the simulated absorption spectra reveals that the permittivity of the Ag film influences the absorption peak greatly at ~500 nm whereas it has ignorable effect on the peak at ~670 nm. A better simulation (blue dot line in Fig. 2a) results from the use of the permittivity of Ag film with a larger imaginary part. Furthermore, the FDTD simulation images were obtained over a domain containing one single semi-sphere with a periodic boundary (Fig. 2b). A normal incident plane wave was applied with the polarization along with X direction. The absorption is insensitive to the polarization of the normally incident light since the semi-sphere Au-NP is symmetric on the X-Y plane[4,12].

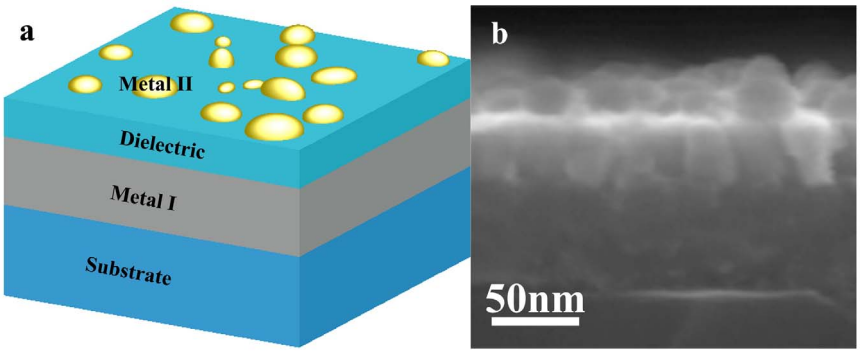

Figure 1 | The construction of PMAs. (a), Illustration of PMAs with random non-prefabricated MNPs. (b), Cross-sectional view of the PMAs with random Au-NPs layer constructed on the ZnO/Ag di-layer structure.

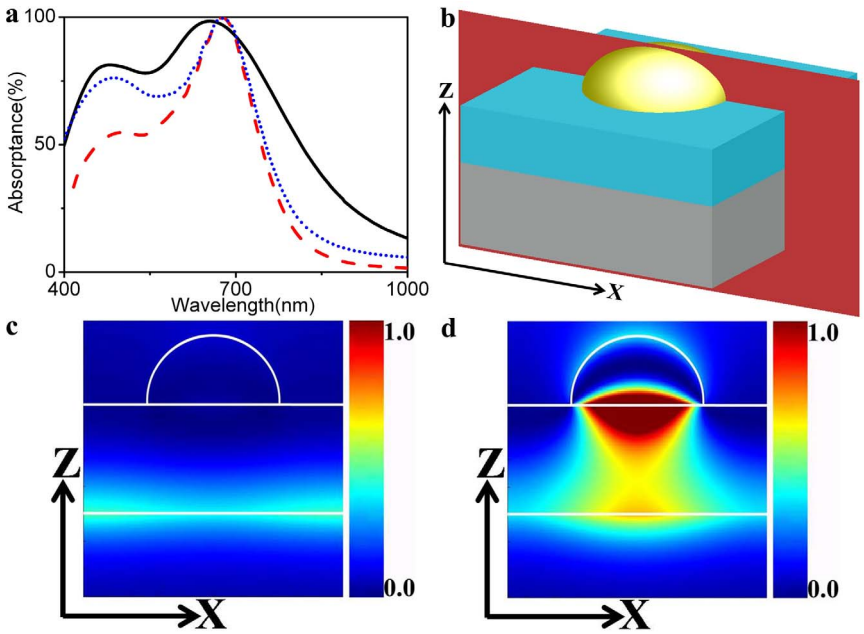

Figure 2 | Experimental and simulation analysis of the PMAs. (a), Absorptance spectra from experiment and numerical simulations with 40 nm ZnO spacer layer. Measured absorptance curve (black solid line), for near normal depolarized incidence (8 degree with respect to surface normal), for random distribution of Au-NPs layer with 22% surface coverage, compared with simulations for normal incidence with polarization along with X direction (see (b)) of uniform, 50 nm in diameter, semispherical Au-NP for periodic boundary (22% surface coverage that the periodic size is 94 nm) with different permittivity of Ag film extracted from the reported work (red dash line) and our experiments (blue dot line). (b), Three dimensional schematic view for simulations of 50 nm semispherical Au-NP showing the cross-section along X-Z plane (red plane). (c), (d), Calculated magnetic field intensities at the peak positions from blue dot line shown in (a) on the X-Z plane as shown in (b) at $\lambda = 487$ nm and $\lambda = 677$ nm, respectively.

We note that the vapor-deposited PMAs were also insensitive to the polarization at the normal incidence case due to random distribution[15,16]. We extracted the magnetic field intensities from the theoretical peaks at 487 nm and 677 nm on the X-Z plane[4]. The uniform magnetic field intensity (Fig. 2c) indicates that the absorption around 487 nm results from the optical interference of the ZnO layer for enhancing Ag absorption. The interaction between the top random Au-NPs and the bottom Ag films (Fig. 2d) results in localized surface plasmon resonance (LSPR)[12,25] or gap plasmon[15] absorption at 677 nm.

In the real vapor-deposited PMAs, the MNPs on the substrate are randomly scattered and have a broad size distribution. Fig. 3 illustrates how the experimental incident angle (8 to 65 degree) affects the absorptance of the vapor-deposited PMAs. Without Au-NPs coating, the bare ZnO-layer-on-Ag-layer (ZnO/Ag) displays an absorption peak (denoted as peak *a*) which is originated from the interference-enhanced absorption of the Ag film (Fig. 3a). Once the resulting PMAs form with the random Au-NPs on the spacer layer, two absorption peaks occur (Fig. 3a). They have a similar variation tendency for the positions of the peak *a* and the peak *b* as the incident angle increases (Fig. 3b) although their intensities are quite different (Fig. 3c). The contrast between the simulation and experiment indicates that the peak *a* and the peak *b* share the same underlying mechanism.

The Au-NPs and gap plasmon have been demonstrated to play an important role for nearly perfect absorption of the vapor-deposited PMAs, which raises the question why the scattering from MNPs is so weak, especially in the resonance cases that the scattering cross section of the nanoparticles should increase dramatically. For MNPs with much smaller size than the wavelength of the excitation wave, the scattering can be generally described as one dipole secondary radiated waves[31]. However, due to an image dipole induced in the

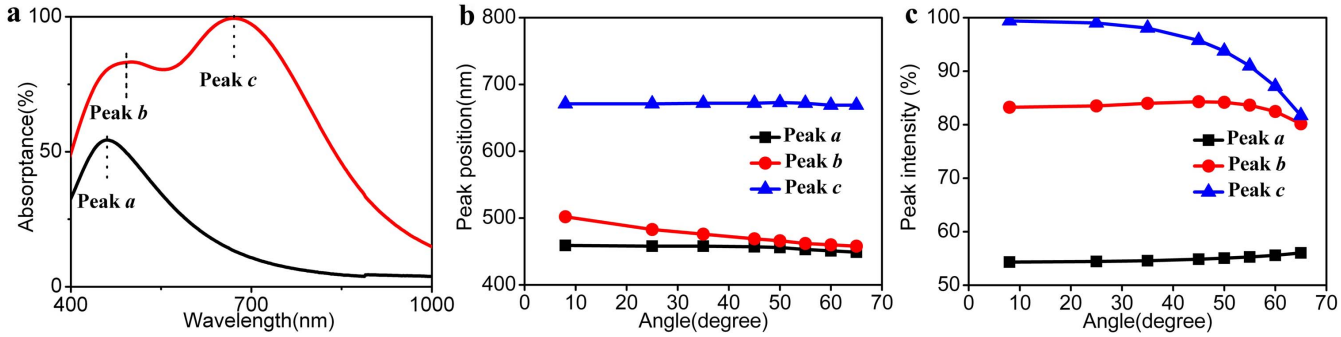

Figure 3 | Incident angle versus measured absorption of the vapor-deposited PMA. (a), Measured absorptance spectra for 8 degree incidence with (red solid line with two maximum values denoted as peak *b* and *c*, respectively) and without (black solid line denoted as peak *a*) random Au-NPs layer (i.e. from 3 nm Au thin film) coated on ZnO/Ag di-layer structure. The ZnO spacer layer is 40 nm in thickness and the random Au-NPs layer is with 22% surface coverage and size distribution in Fig. S1c. (b), (c), Peak position and peak intensity of the peak *a*, *b*, *c* as a function of the incident angle, respectively.

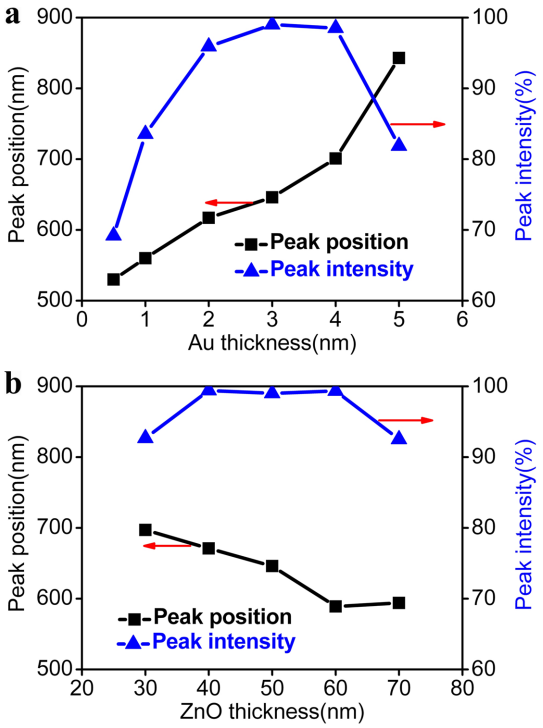

Figure 4 | Tunable absorption of the vapor-deposited PMAs. (a), Position and intensity of the peak *c* as a function of the deposited Au film thickness with ZnO spacer layer keeping 50 nm in thickness. (b), Position and intensity of the peak *c* versus the ZnO space layer thickness while the thickness of deposited Au film stay in 3 nm.

bottom Ag film with an opposite dipole moment when the polarization is parallel to the Ag film surface[32], the scattering from the MNPs is suppressed. The scattering cross section is about sixth power of the real particle sizes while the absorption cross section is only about third power[31]. The scattering effect weakens rapidly as the size of the MNPs decreased while absorbing, instead of scattering is dominantly responsible for the extinction of the incident light. On the other hand, the scattering effects reduce further due to the destructive interference of the scattering waves, or that the average surface roughness is much smaller than the characteristic wavelength[3]. All these were evidenced by the evaluations on the average surface roughness and the comparison between the reflections (Fig. S2).

Extracted from Eq. 1, the effective impedance z_{eff} is dependent on the intrinsic properties of both materials and constructed architectures (See SI), and can be described as $z_{eff} = \sqrt{\mu_{eff}/\varepsilon_{eff}} = G(z_1, z_d, z_{II}^{eff}, h_{eff}, d)$. ε_{eff} and μ_{eff} are effective permittivity and permeability of the PMAs fabricated, respectively. z_1 and z_d are the impedance of the bottom metal film and the dielectric spacer layer, respectively, while h_{eff} is the effective thickness of the metal II layer and d is the thickness of dielectric layer. z_{II}^{eff} is the effective impedance of the metal II layer, and related to the surface coverage, size distribution and effective polarizability of the metal II nanoparticles. Combined with Eq. 1, the reflection of the vapor-deposited PMA is strongly dependent on h_{eff} and z_{II}^{eff} of the top Au-NPs layer, and z_d and d of the dielectric spacer layer. Thus, on the basis of tunable vapor deposition process, we can flexibly control the position of the absorption peak through these above-motioned parameters. In Fig. 4, we show how the thickness of both the dielectric spacer layer (Fig. 4a) and the Au film deposited to form the Au-NPs (Fig. 4b) affects the position and the intensity of the measured absorption peaks of the vapor-deposited PMAs. The absorption reaches over 99% and the absorption peak position varies from ~590 nm to ~670 nm when the spacer layer thickness is changed from 40 nm to 60 nm. When the Au film is 3 nm thick prior to annealing, the absorptance could reach up to 99%.

Besides, most traditional PMAs are only fabricated on flat substrates because of the fabrication limitation on any arbitrary structured substrates. The vapor deposition can allow greater control on any desirable surfaces. The PMAs on rough surface have been designed and fabricated as shown in Fig. 5. This construction delivers a very broad and nearly reflectionless band with a reflectance of less than 1%, which is beneficial for the PMAs. The vapor deposition seems to be a versatile method that can be incorporated into the direct fabrication of PMAs. The vapor-deposited PMAs require neither lithographical processes for ordered structures nor prefabrication processes for metal colloids. The option of using the spacer layer and/or the top MNPs, the simplified architecture, and the availability of other metals and dielectrics that could form PMAs provide one with a unique laboratory in which PMAs can be realized for selected wavelengths (Fig. S3).

We demonstrated controllable 'amorphous' metamaterials with disordered non-prefabricated MNPs for achieving visible PMAs by means of the CMOS-compatible ALD dielectric layer and random non-prefabricated MNPs. Our concept and analysis reveals that the large-area visible-PMAs can be achieved by using an vapor deposited dielectric layer and a monolayer of MNPs on any arbitrary structured substrates. Whether vapor deposition emerges as the preferred route for manufacture or simply represents a bench mark method for constructing the controlled-reflectance surfaces without ordered nanostructures remains to be seen. The vapor-deposited controlled-reflectance surface or the tunable PMA is now compatible with those lithographical and self-assembly technologies, and is

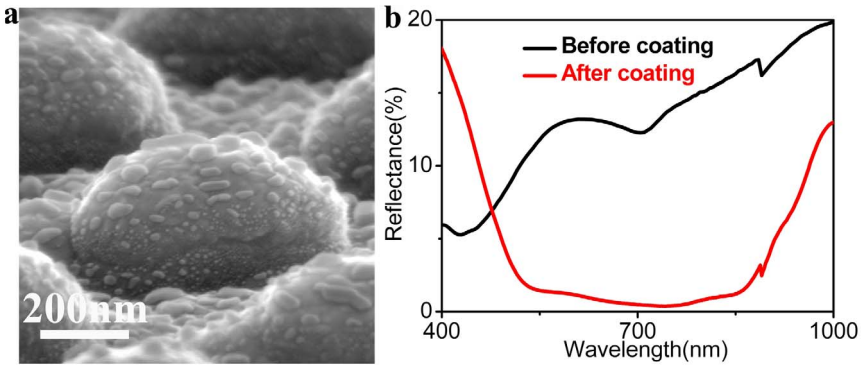

Figure 5 | PMA fabricated on structured substrates. (a), Top view (60 degree angle of the view) of the PMA fabricated on a structured surface by vapor-deposited with 100 nm Ag bottom layer, 40 nm ZnO space layer and 4 nm Au film deposited for Au-NPs. (b), The measured reflectance spectra for near normal depolarized incident, of the structured surface (black solid line) and PMA@surface (red solid line).

hence likely to be adopted by the PMA community with the potential applications in solar cells, thermal emitter and sensors. The controlled-reflectance surface or the tunable PMA containing a monolayer of disordered structures will stimulate theoretical interests in the underline physics behind amorphous metamaterials and even disordered photonics in ideal absorbers.

Methods

With a simple vapor-deposited planar sandwiched film which incorporates a bottom silver film, a spacer layer of nanoscale-thick oxide and a top layer of random non-prefabricated Au-NPs formed by annealing. The continuous Ag thin film was deposited by argon ion beam sputtering on Silicon substrate. The ZnO dielectric layer was then deposited on the Ag thin film by ALD with an atom scale controllable thickness[26,27] at 190°C. Then, an Au thin film, also with a controllable thickness, was sputtered on the dielectric layer to form Au/ZnO/Ag sandwich structure by sputtering coating. At last, we annealed the prepared Au/ZnO/Ag sandwich structure for transforming the top Au film lay into Au-NPs at 300°C for 30 minutes.

1. Ebbesen, T. W., Lezec, H. J., Ghaemi, H. F., Thio, T. & Wolff, P. A. Extraordinary optical transmission through sub-wavelength hole arrays. *Nature* **391**, 667–669 (1998).
2. Landy, N. I., Sajuyigbe, S., Mock, J. J., Smith, D. R. & Padilla, W. J. Perfect metamaterial absorber. *Phys. Rev. Lett.* **100**, 207402 (2008).
3. Watts, C. M., Liu, X. & Padilla, W. J. Metamaterial electromagnetic wave absorbers. *Adv. Mater.* **24**, OP98–OP120 (2012).
4. Hao, J., Zhou, L. & Qiu, M. Nearly total absorption of light and heat generation by plasmonic metamaterials. *Phys. Rev. B* **83**, 165107 (2011).
5. Sun, S. *et al*. Gradient-index meta-surfaces as a bridge linking propagating waves and surface waves. *Nature Mater.* **11**, 426–431 (2012).
6. Landy, N. I. *et al*. Design, theory, and measurement of a polarization-insensitive absorber for terahertz imaging. *Phys. Rev. B* **79**, 125104 (2009).
7. Smith, D. R., Padilla, W. J., Vier, D. C., Nemat-Nasser, S. C. & Schultz, S. Composite medium with simultaneously negative permeability and permittivity. *Phys. Rev. Lett.* **84**, 4184–4187 (2000).
8. Shelby, R. A., Smith, D. R. & Schultz, S. Experimental verification of a negative index of refraction. *Science* **292**, 77–79 (2001).
9. Smith, D. R., Pendry, J. B. & Wiltshire, M. C. K. Metamaterials and negative refractive index. *Science* **305**, 788–792 (2004).
10. Shalaev, V. M. Optical negative-index metamaterials. *Nature Photon.* **1**, 41–48 (2007).
11. Pendry, J. B. Negative refraction makes a perfect lens. *Phys. Rev. Lett.* **85**, 3966–3969 (2000).
12. Liu, N., Mesch, M., Weiss, T., Hentschel, M. & Giessen, H. Infrared perfect absorber and its application as plasmonic sensor. *Nano Lett.* **10**, 2342–2348 (2010).
13. Liu, X., Starr, T., Starr, A. F. & Padilla, W. J. Infrared spatial and frequency selective metamaterial with near-unity absorbance. *Phys. Rev. Lett.* **104**, 207403 (2010).
14. Schurig, D. *et al*. Metamaterial electromagnetic cloak at microwave frequencies. *Science* **314**, 977–980 (2006).
15. Moreau, A. *et al*. Controlled-reflectance surfaces with film-coupled colloidal nanoantennas. *Nature* **492**, 86–89 (2012).
16. Hägglund, C. *et al*. Self-assembly based plasmonic arrays tuned by atomic layer deposition for extreme visible light absorption. *Nano Lett.* **13**, 3352–3357 (2013).
17. Vardeny, Z. V., Nahata, A. & Agrawal, A. Optics of photonic quasicrystals. *Nature Photon.* **7**, 177–187 (2013).
18. Bravo-Abad, J., Fernández-Domínguez, A. I., García-Vidal, F. J. & Martín-Moreno, L. Theory of extraordinary transmission of light through quasiperiodic arrays of subwavelength holes. *Phys. Rev. Lett.* **99**, 203905 (2007).
19. Pacifici, D., Lezec, H. J., Sweatlock, L. A., Walters, R. J. & Atwater, H. A. Universal optical transmission features in periodic and quasiperiodic hole arrays. *Opt. Express* **16**, 9222–9238 (2008).
20. Dal Negro, L. & Boriskina, S. V. Deterministic aperiodic nanostructures for photonics and plasmonics applications. *Laser Photon. Rev.* **6**, 178–218 (2012).
21. Wiersma, D. S. Disordered photonics. *Nature Photon.* **7**, 188–196 (2013).
22. Hedayati, M. K. *et al*. Design of a perfect black absorber at visible frequencies using plasmonic metamaterials. *Adv. Mater.* **23**, 5410–5414 (2011).
23. Hedayati, M. K., Faupel, F. & Elbahri, . M. Tunable broadband plasmonic perfect absorber at visible frequency. *Appl. Phys. A* **109**, 769–773 (2012).
24. Chen, X. *et al*. Near-infrared broadband absorber with film-coupled multilayer nanorods. *Opt. Lett.* **38**, 2247–2249 (2013).
25. Yan, M., Dai, J. & Qiu, M. Lithography-free broadband visible light absorber based on a mono-layer of gold nanoparticles. *J. Opt.* **16**, 025002 (2014).
26. George, S. M. Atomic Layer Deposition: An Overview. *Chem. Rev.* **110**, 111–131 (2009).
27. Zhang, Y. *et al*. Near-perfect infrared absorption from dielectric multilayer of plasmonic aluminum-doped zinc oxide. *Appl. Phys. Lett.* **102**, 213117 (2013).
28. Engheta, N. Thin absorbing screens using metamaterial surfaces. *Antennas and Propag. Soc. Int. Symp, 2002 IEEE.* **2**, 392–395 (2002).
29. Johnson, P. B. & Christy, R. W. Optical constants of the noble metals. *Phys. Rev. B* **6**, 4370–4379 (1972).
30. Zhang, S. *et al*. Demonstration of metal-dielectric negative-index metamaterials with improved performance at optical frequencies. *J. Opt. Soc. Am. B* **23**, 434–438 (2006).
31. Bohren, C. F. & Huffman, D. R. *Absorption and scattering of light by small particles* (John Wiley & Sons, Inc, 1983).
32. Mock, J. J. *et al*. Distance-dependent plasmon resonant coupling between a gold nanoparticle and gold film. *Nano Lett.* **8**, 2245–2252 (2008).

Acknowledgments

The authors thank T.N. Zhang, J. Shao, L. Zhu for helpful discussion and technical supporting. This work was funded by National Basic Research Program of China (2012CB934301 and 2011CBA00905), NSFC (61376016, 61290304, and 61275114) and CAS.

Author contributions

Y.Z., C.X. and N.D. performed the design, experiments, theoretical simulations and analysis, and wrote the manuscript. T.X.W. and W.J.D. contributed the ALD process and spectroscopy measurements. K.N.Z. and Y.S. contributed to the deposition of Au and Ag films and the SEM measurements.

Additional information

Supplementary information accompanies this paper at http://www.nature.com/scientificreports

Competing financial interests: The authors declare no competing financial interests.

How to cite this article: Zhang, Y. *et al*. Vapor-deposited amorphous metamaterials as visible near-perfect absorbers with random non-prefabricated metal nanoparticles. *Sci. Rep.* **4**, 4850; DOI:10.1038/srep04850 (2014).